

A Lower Angular Momentum Limit for Self-Gravitating Protostellar Disc Fragmentation

Duncan Forgan^{1*} and Ken Rice¹

¹*Scottish Universities Physics Alliance (SUPA), Institute for Astronomy, University of Edinburgh, Blackford Hill, Edinburgh, EH9 3HJ, Scotland, UK*

Accepted

ABSTRACT

We attempt to verify recent claims (made using semi-analytic models) that for the collapse of spherical homogeneous molecular clouds, fragmentation of the self-gravitating disc that subsequently forms can be predicted using the cloud’s initial angular momentum alone. In effect, this condition is equivalent to requiring the resulting disc be sufficiently extended in order to fragment, in line with studies of isolated discs. We use smoothed particle hydrodynamics with hybrid radiative transfer to investigate this claim, confirming that in general, homogeneous spherical molecular clouds will produce fragmenting self-gravitating discs if the ratio of rotational kinetic energy to gravitational potential energy is greater than $\approx 5 \times 10^{-3}$, where this result is relatively insensitive to the initial thermal energy. This condition begins to fail at higher cloud masses, suggesting that sufficient mass at large radii governs fragmentation. While these results are based on highly idealised initial conditions, and may not hold if the disc’s accretion from the surrounding envelope is sufficiently asymmetric, or if the density structure is perturbed, they provide a sensible lower limit for the minimum angular momentum required to fragment a disc in the absence of significant external turbulence.

Key words: stars: formation, accretion, accretion discs, methods: numerical, radiative transfer, hydrodynamics

1 INTRODUCTION

Cold, dense molecular cloud cores are thought to be the sites of low-mass star formation (Terebey et al. 1984). Typically, these cores will contain an excess of angular momentum (compared with the rotational angular momentum of low-mass stars, cf Caselli et al. 2002). If these cores are sufficiently dense, they will collapse under their own gravity to form a protostar plus protostellar disc, with a substantial envelope surrounding both. In this pre-main sequence phase, we can expect that most of the star’s eventual mass will be processed by the protostellar disc (which in turn accretes this mass from a surrounding envelope).

The star’s accretion is inextricably linked with the process of outward angular momentum transport - understanding the mechanisms by which angular momentum transport functions in these early phases is therefore essential to theories of star formation. While turbulence induced by the magneto-rotational instability (MRI) defines angular momentum transport at late times (Blaes & Balbus 1994; Balbus & Papaloizou 1999), the disc is unlikely to be even weakly ionised at early times. We must therefore seek another means by which to generate angular momentum transport.

Simulations suggest that the disc is likely to be self-

gravitating at these early times, as the disc mass will be large relative to the star mass (Bate 2010; Machida & Matsumoto 2011). If the disc becomes gravitationally unstable, this may provide the dominant transport mechanism through the growth of self-regulated gravito-turbulence (Boss 1984; Lin & Pringle 1987; Laughlin & Bodenheimer 1994). A self-gravitating disc will become subject to gravitational instability (GI) if the Toomre parameter, Q (Toomre 1964):

$$Q = \frac{c_s \kappa}{\pi G \Sigma} \sim 1, \quad (1)$$

where c_s is the sound speed, Σ is the surface density, and κ is the epicyclic frequency (in the case of a Keplerian disc, κ is equal to the angular frequency Ω). If $Q < 1$, axisymmetric perturbations will grow within the disc. Numerical simulations have established that discs with $Q < 1.5 - 1.7$ will be unstable to non-axisymmetric perturbations (Durisen et al. 2007). The onset of GI is accompanied by the growth of quasi-steady spiral structures, which drive shocks with Mach numbers of order unity (Cossins et al. 2009).

The growth of GI in a self-gravitating disc will generally lead to a state commonly referred to as marginal instability (Paczynski 1978), where the heating due to GI is balanced by radiative cooling. The combination of these two processes produces a quasi-equilibrium state where the instability’s amplitudes are modulated, providing a self-regulated outward angular momentum transport process (Gammie 2001; Pickett et al.

* E-mail: dhf@roe.ac.uk

2 Duncan Forgan and Ken Rice

2003; Lodato & Rice 2004; Cai et al. 2008). The growth and decay of these structures provides the so-called gravito-turbulence, allowing the evolution of the disc to be described in a pseudo-viscous fashion (e.g. Balbus & Papaloizou 1999; Lodato & Rice 2004; Rice & Armitage 2009; Clarke 2009), where the transport can be characterised using the dimensionless turbulent viscosity parameter α (Shakura & Sunyaev 1973). While this local α -parametrisation breaks down in certain limits (Forgan et al. 2011), it remains a useful tool to compare to other transport mechanisms such as the MRI.

Self-gravitating disc evolution is also an important component of planet formation theory, not merely through its effects on the growth and accretion of planetary cores (Rice et al. 2004; Clarke & Lodato 2009). If the disc is self-gravitating, its dynamical evolution can rapidly form giant planets and brown dwarfs by disc fragmentation (Kuiper 1951; Boss 1997; Stamatellos et al. 2007). While the Q criterion is a necessary condition for disc fragmentation, it is insufficient. A second criterion is required, relating to the local cooling time:

$$t_{\text{cool}} = \frac{u}{du/dt}, \quad (2)$$

where u is the specific internal energy. It is often more suitable to discuss cooling in terms of a dimensionless parameter, β_c :

$$\beta_c = t_{\text{cool}}\Omega. \quad (3)$$

Gammie (2001) showed using shearing-sheet simulations that if $\beta_c = \text{const.}$, fragmentation can only occur if $\beta_c < \beta_{\text{crit}}$, where β_{crit} is approximately 3, although it was later shown that β_{crit} depends on the local equation of state, in particular the value of the ratio of specific heats, γ (Rice et al. 2005). The correct values of $\beta_{\text{crit}}(\gamma)$ have been challenged by recent work, and may be slightly higher (Meru & Bate 2011a; Paardekooper et al. 2011). In the case of smoothed particle hydrodynamics (SPH) simulations as are carried out in this work, this appears to be due to resolution effects pushing the convergence limit to higher particle number than was previously anticipated (Lodato & Clarke 2011), as well as possible issues regarding the correct implementation of cooling prescriptions (Rice, Forgan and Armitage, submitted).

Alternatively, the second fragmentation criterion can be couched in terms of the local stresses in the disc. In the Shakura-Sunyaev formalism, the effective turbulent viscosity $\nu = \alpha c_s H$, where H is the disc scale height. Stresses have two principal origins in self-gravitating discs¹ - Reynolds stresses (induced by correlated velocity perturbations) and gravitational stresses (induced by correlated perturbations in the gravitational potential). Assuming that the disc is in thermal equilibrium, the value of α can be determined by balancing the pseudo-viscous heating and the radiative cooling:

$$\alpha_{\text{cool}} = \left(\frac{d \ln \Omega}{d \ln r} \right)^{-2} \frac{1}{\gamma(\gamma - 1)\beta_c}. \quad (4)$$

Rice et al. (2005) show that a single critical value of $\alpha = \alpha_{\text{crit}} \approx 0.06$ can be used as the second fragmentation criterion, for any value of γ . If the disc is irradiated, it has been shown that α , does not uniquely determines the likelihood of fragmentation, and that short cooling times can induce fragmentation even in low-stress environments (Rice et al. 2011). Studies have however shown that this α_{crit} value may not apply if β_c can vary

(Clarke et al. 2007), or if the disc's accretion from the envelope is substantial (Kratter et al. 2008; Harsono et al. 2011). In these circumstances, more sophisticated criteria are required (see e.g. Forgan & Rice 2011). In spite of these circumstances, it has been established by many authors that the requisite conditions for fragmentation only occur in the outer regions of discs (Rafikov 2005; Matzner & Levin 2005; Whitworth & Stamatellos 2006; Boley et al. 2006; Stamatellos & Whitworth 2008; Forgan et al. 2009; Clarke 2009; Rice et al. 2010). These results hold in semi-analytic calculations, grid-based simulations and particle-based simulations. This does not limit the usefulness of disc fragmentation as an explanation for observable exoplanets - indeed, it explains the properties of systems such as HR 8799 when core accretion theories struggle to do so (Kratter et al. 2010; Nero & Bjorkman 2009). Meru & Bate (2011b) presented SPH simulations which displayed inner disc fragmentation for steep surface density profiles, but it has been shown that these can be explained by failure to address resolution criteria relating to the artificial viscosity (Lodato & Clarke 2011) - indeed, a failure that all previous SPH simulations of this type have shared.

As has been stated, the self-gravitating phase is expected to occur at early times, when the disc is still embedded in the envelope. Therefore, to fully understand the fragmentation of self-gravitating discs, it is necessary to include the envelope's contribution, both in its ability to supply the disc with matter (Kratter et al. 2008), and in the resulting stresses it can induce at the disc's surface and beyond (Harsono et al. 2011). These stresses result in extensive non-local angular momentum transport, a phenomenon which will tend to invalidate semi-analytic models (Forgan et al. 2011).

A straightforward means by which the envelope can be included is to begin with a rotating molecular cloud as initial conditions. Frequently, the cloud parameters ϕ and λ are used² where:

$$\phi = \frac{E_{\text{therm}}}{E_{\text{grav}}} \quad (5)$$

$$\lambda = \frac{E_{\text{rot}}}{E_{\text{grav}}}, \quad (6)$$

where E_{therm} , E_{rot} and E_{grav} are the cloud's total thermal, rotational and gravitational energies respectively. For an initially isothermal cloud in rigid body rotation, these parameters essentially define the cloud's initial temperature and angular velocity:

$$\phi = \frac{5kT_0 R_{\text{cl}}}{2\mu m_H G M_{\text{cl}}} \quad (7)$$

$$\lambda = \frac{\Omega_0^2 R_{\text{cl}}^3}{3G M_{\text{cl}}}, \quad (8)$$

where R_{cl} is the cloud's initial radius, k is Boltzmann's constant, μ is the mean molecular weight of the gas and m_H is the mass of the hydrogen atom. Tohline (1981) considers the collapse of adiabatic spheroids ($P = K\rho^\Gamma$), and defines a series of criteria for these clouds to become unstable to nonaxisymmetric perturbations, dependent on the polytropic index Γ of the cloud:

$$\phi \leq \begin{cases} 0.109 \lambda^{-1} & \Gamma = 1 \\ 0.201 & \Gamma = 4/3 \\ 0.228 \lambda^{0.2} & \Gamma = 7/5 \\ 0.372 \lambda & \Gamma = 5/3. \end{cases} \quad (9)$$

¹ A third source of disc stress is magnetic fields, but as the self-gravitating phase is typically very weakly ionised, the magnitude of these stresses is small, and hence we do not consider them here

² In the literature, these parameters are known as α and β respectively. We relabel them to avoid confusion with the subsequent disc parameters.

In reality, a collapsing molecular cloud will have a more complex thermal history that requires a more detailed understanding of the equation of state as a function of the local density and temperature. Rice et al. (2010), using a model initially developed by Lin & Pringle (1990), carried out semi-analytic calculations of uniform, spherical molecular cloud collapse, with a more complex equation of state, using the pseudo-viscous approximation to evolve the resulting disc, which continues to accrete from its envelope. They show that the resulting self-gravitating discs are subject to fragmentation (i.e. they contain regions where $\alpha_{\text{cool}} > 0.06$) when $\lambda > 1 \times 10^{-3}$, and never fragment when $\lambda \leq 1 \times 10^{-3}$, *regardless of the initial thermal energy of the cloud*.

It is not clear whether these results can be expected to hold, given that non-local angular momentum transport (which must play a role, especially at early times) is not accounted for, as well as potentially asymmetric accretion flows. In addition, these initial conditions are extremely simple, and not likely to be reproduced in reality - a more appropriate choice would be supercritical Bonnor-Ebert spheres (e.g. Walch et al. 2009), as well as the addition of turbulence (Walch et al. 2010). Finally, as has been previously stated, using $\alpha_{\text{crit}} = 0.06$ is probably not appropriate for accreting discs.

We aim to perform a set of numerical experiments using smoothed particle hydrodynamics with hybrid radiative transfer (Forgan et al. 2009) to appraise the validity of the angular momentum condition set forth by Rice et al. (2010). Unlike Walch et al. (2009), we do not hold ϕ constant, and therefore we can also detect whether any dependence on thermal energy exists. Also, we can model non-local angular momentum transport, and can measure fragmentation directly rather than relying on uncertain criteria, allowing us to test more reliably whether an angular momentum criterion truly exists.

2 METHOD

2.1 SPH and the Hybrid Radiative Transfer Approximation

Smoothed Particle Hydrodynamics (SPH) (Lucy 1977; Gingold & Monaghan 1977; Monaghan 1992) is a Lagrangian formalism that represents a fluid by a distribution of particles. Each particle is assigned a mass, position, internal energy and velocity. State variables such as density and pressure are then calculated by interpolation (see reviews by Monaghan 1992, 2005). In the simulations presented here, the gas is modelled using 500,000 SPH particles while the star is represented by a point mass particle onto which gas particles can accrete, if they are sufficiently close (in our case, within 1 au) and are bound (Bate et al. 1995). An SPH particle is converted to a pointmass if the local density has exceeded $10^{-12} \text{ g cm}^{-3}$, and

- (i) There exists one Jeans mass within the particle's neighbour sphere
- (ii) The neighbour sphere is bound (i.e. the total energy inside the sphere is negative)
- (iii) The local gravitational potential energy exceeds both the thermal and rotational kinetic energy

The SPH code used in this work is based on the SPH code developed by Bate et al. (1995) which uses individual particle timesteps, and individually variable smoothing lengths, h_i , such that the number of nearest neighbours for each particle is 50 ± 20 . The code uses a hybrid method of approximate radiative transfer (Forgan et al. 2009), which is built on two pre-

existing radiative algorithms: the polytropic cooling approximation devised by Stamatellos et al. (2007), and flux-limited diffusion (e.g., Whitehouse & Bate 2004; Mayer et al. 2007, see Forgan et al. 2009 for details). This union allows the effects of both global cooling and radiative transport to be modelled, without imposing extra boundary conditions.

The opacity and temperature of the gas is calculated using a non-trivial equation of state. This accounts for the effects of H_2 dissociation, H^0 ionisation, He^0 and He^+ ionisation, ice evaporation, dust sublimation, molecular absorption, bound-free and free-free transitions and electron scattering (Bell & Lin 1994; Boley et al. 2007; Stamatellos et al. 2007). Heating of the disc is also achieved by $P dV$ work and shock heating.

2.2 Initial Cloud Conditions

The molecular clouds were initialised with 500,000 SPH particles. While this may seem under-resolved in the light of the results from Meru & Bate (2011a), it is important to note that they use a fundamentally different cooling method where particle cooling rates are not affected by their neighbours. The hybrid method, through its flux limited diffusion component, does account for the neighbour sphere. A more appropriate resolution criterion (Lodato & Clarke 2011, based on the results of Meru & Bate 2011a) shows that 500,000 particles is sufficient to resolve fragmentation, and is discussed in the following section. The particles were distributed in a sphere with uniform density. The clouds were initialised with varying values of cloud mass M_{cl} and λ - the cloud radii R_{cl} were specified in order to maintain the same initial density $\rho_0 = 1.46 \times 10^{-17} \text{ g cm}^{-3}$. This ensures that all clouds have the same free-fall time

$$t_{\text{ff}} = \sqrt{\frac{3\pi}{32G\rho_0}} = 1.74 \times 10^4 \text{ yr.} \quad (10)$$

The initial cloud temperature is fixed at 5 K, equal to the background temperature (beyond which the cloud cannot cool). Note by fixing the parameters in this fashion, we allow ϕ to vary. We choose this setup as it is similar to that of the semi-analytic calculations of Rice et al. (2010), who also allow ϕ to vary in this fashion. Their results appear to be independent of ϕ , and we wish to assess if this is true in our case. We do not apply a density perturbation to the clouds, as is often done in simulations of this type (e.g. Boss 1986). The amplitude of the $m = 2$ mode initially is zero in our simulations - the subsequent growth of $m = 2$ spiral modes is purely a result of disc torques forming from gravitational instabilities.

2.3 Resolution Conditions

To ensure that potential fragmentation is resolved, the minimum resolvable Jeans mass - one neighbour group of SPH particles (Bate & Burkert 1997), around 50 in the case of the code used - must be sufficiently small:

$$M_{\text{min}} = 2N_{\text{neigh}}m_i = 2M_{\text{tot}}\frac{N_{\text{neigh}}}{N_{\text{tot}}}. \quad (11)$$

The minimum resolvable Jeans mass ranges between $33M_{\oplus}$ for $M_{\text{cl}} = 0.5M_{\odot}$ to $120M_{\oplus}$ for $M_{\text{cl}} = 2M_{\odot}$. As it is expected that fragment masses will be typically several orders of magnitude higher than these values (Kratte et al. 2010; Forgan & Rice 2011), this establishes that the simulations would comfortably resolve disc fragmentation if it were to occur.

Table 1. Summary of the cloud parameters investigated in this work.

Simulation	$M_{\text{cl}} (M_{\odot})$	$R_{\text{cl}} (\text{au})$	λ	ϕ
1	1.0	2133.33	4×10^{-3}	0.2
2	1.0	2133.33	5×10^{-3}	0.2
3	1.0	2133.33	6×10^{-3}	0.2
4	1.0	2133.33	7×10^{-3}	0.2
5	1.0	2133.33	8×10^{-3}	0.2
6	1.0	2133.33	9×10^{-3}	0.2
7	0.5	1693.23	4×10^{-3}	0.4
8	0.5	1693.23	5×10^{-3}	0.4
9	0.5	1693.23	6×10^{-3}	0.4
10	0.5	1693.23	7×10^{-3}	0.4
11	0.5	1693.23	8×10^{-3}	0.4
12	0.5	1693.23	9×10^{-3}	0.4
13	2.0	2687.83	4×10^{-3}	0.1
14	2.0	2687.83	5×10^{-3}	0.1
15	2.0	2687.83	6×10^{-3}	0.1
16	2.0	2687.83	7×10^{-3}	0.1
17	2.0	2687.83	8×10^{-3}	0.1
18	2.0	2687.83	9×10^{-3}	0.1

Perhaps more important are the resolution issues raised by artificial viscosity (Lodato & Clarke 2011). While required by the SPH code, this artificial viscosity must be quantified so that we know where in the disc the artificial viscosity is likely to be lower than the effective viscosity generated by the gravitational instabilities. If the stress induced by artificial viscosity exceeds that of the stresses induced by the gravitational instability in some region of the disc, then fragmentation is likely to be suppressed (Whitworth 1998).

The linear term for the artificial viscosity can be expressed as (Artymowicz & Lubow 1994; Murray 1996; Lodato & Price 2010)

$$\nu_{\text{art}} = \frac{1}{10} \alpha_{\text{SPH}} c_s h, \quad (12)$$

where c_s is the local sound speed, h is the local SPH smoothing length, and α_{SPH} is the linear viscosity coefficient used by the SPH code (taken to be 0.1). We can define an effective α parameter associated with the artificial viscosity (Lodato & Rice 2004; Forgan et al. 2011)

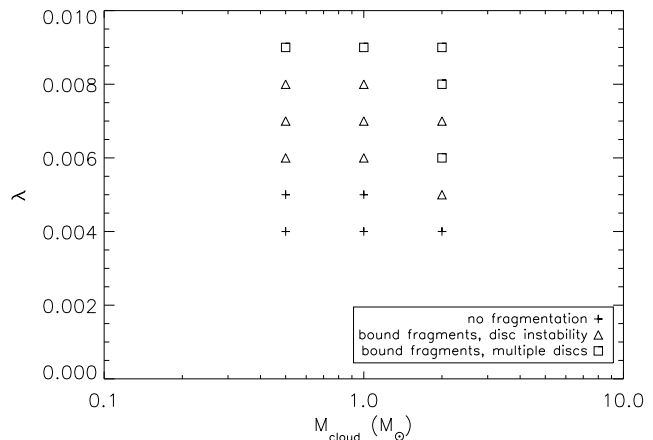
$$\nu_{\text{art}} = \alpha_{\text{art}} c_s H, \quad (13)$$

and hence combining equations (12) and (13) gives (Artymowicz & Lubow 1994; Murray 1996; Lodato & Price 2010)

$$\alpha_{\text{art}} = \frac{1}{10} \alpha_{\text{SPH}} \frac{h}{H}. \quad (14)$$

This shows that where the vertical structure is not well resolved (i.e., $\frac{h}{H}$ is large), artificial viscosity will dominate. In the simulations presented here, this is likely to be the case inside ~ 10 au, so any data inside this region can not be used. We therefore only consider results outside this radius, and therefore cannot comment on works which demonstrate fragmentation inside this radius. In the regions where fragmentation is found, the artificial viscosity is less than 1% of the total, and therefore satisfies the ‘‘less than 5%’’ criterion given by Lodato & Clarke (2011) for correctly resolving fragmentation.

Finally, we must recognise that these simulations contain Poisson noise in the initial conditions. After approximately one free-fall

**Figure 1.** The fragmentation boundary in the simulations conducted. The boundary between disc fragmentation and no fragmentation depends only weakly on initial cloud mass.

time, the star-disc system begins to settle into a marginally unstable state, effectively erasing the initial conditions. Fragmentation due to disc instability typically takes an extra $0.5t_{\text{ff}}$ after disc formation, corresponding to many outer rotation periods (ORPs), so we do not expect this initial noise to significantly alter our result. To confirm this, all simulations were repeated, using a different set of randomly generated initial conditions, to confirm that this initial noise does not affect the final result.

3 RESULTS

3.1 General Trends

Each of the clouds goes through a set of generic evolutionary phases, similar in nature to those described by Masunaga & Inutsuka (2000) for a non-rotating homogeneous cloud. Initially, the collapse is isothermal - despite the central density increasing by several orders of magnitude, the central temperature remains constant at the background temperature of 5K. As the central density increases past $10^{-12} \text{ g cm}^{-3}$, the gas becomes optically thick, and the central temperature begins to rise. As the temperature rises, rotational degrees of freedom in H_2 are activated, and the contraction slows somewhat as the cloud develops significant thermal pressure support, forming the ‘‘first core’’ (cf Larson 1969). As these simulations contain a sufficient amount of initial angular momentum, this oblate first core will subsequently form the protostellar disc (Machida & Matsumoto 2011). This process begins with the formation of a bar within the core, which decays into spiral structures (cf Bate 2010). The second core forms at the centre of this disc structure at approximately 2000 K, when H_2 begins to dissociate, removing thermal energy and hence pressure support. At this stage, the simulation forms a pointmass. The disc-to-pointmass mass ratio is initially larger than 3, and the star accretes rapidly. After this rapid accretion phase, the mass ratio drops below unity, and the marginally unstable self-gravitating phase begins (except in the simulations that produce multiple discs).

Figure 1 displays the end state of all the simulations run in this work. The end states can be categorised into one of three broad classes:

- (i) Non-fragmenting, marginally unstable self-gravitating discs, (denoted by ‘+’ in Figure 1),

(ii) Self-gravitating discs which fragment several ORPs after formation (denoted by triangles in Figure 1),

(iii) Systems which fragment into multiple systems before a single disc system can form (denoted by squares in Figure 1).

It can be seen that the delineation of the three classes shows only a very weak dependence on the initial cloud mass M_{cl} . Note that all clouds have the same initial free-fall time, and the same external background temperature. The clouds are initially isothermal, and will therefore cool quickly to the background temperature, removing any dependence on initial thermal energy (unlike the adiabatic clouds of for example Tohline 1981) The fact that initial angular momentum provides a (relatively) simple criterion

$$\lambda > 5 \times 10^{-3} \quad (15)$$

(and its subsequent weak violation at larger cloud masses) suggests that fragmentation requires placing a sufficient quantity of material at large radii at early times, having the resulting effect of reducing the Q parameter without triggering a strong increase in the local cooling time. This allows sufficient stress to be generated as a result of the gravitational instability, which fragments the disc. Our results contrast with those from simulations where an azimuthal density perturbation is applied, for example Boss (1986), who find that binary formation occurs at $\lambda = 4 \times 10^{-3}$. This discrepancy seems reasonable again under the interpretation of sufficient mass at large radii at early times promoting fragmentation.

Discs which do not fragment are qualitatively different in their properties to discs that do. These differences are generic to all initial cloud masses. For the sake of brevity, we will only explore the $M_{cl} = 1M_{\odot}$ clouds in detail.

3.2 The $M_{cl} = 1M_{\odot}$ Simulations

3.2.1 General Properties

Figure 2 shows surface density plots for Simulations 1, 2, 3, 4, 5 and 6, after at least $2t_{ff}$ of evolution, or during fragmentation in the case of Simulations 3, 4, 5 and 6. In Simulations 3, 4 and 5, fragmentation occurs around $t = 1.5t_{ff}$, in Simulation 6 it occurs around $t = 1t_{ff}$. It is clear that increasing the initial cloud angular momentum increases the overall disc extent. There is also a general tendency for fragments to form closer to the central object as the angular momentum is increased. In all cases, it is apparent that the spiral structure is dominated by $m = 2$ spiral modes - we shall return to the nature of their angular momentum transport in the following sections.

Figure 3 shows azimuthally averaged radial profiles for Simulations 1, 2, 3, 4 and 5. The impact of increasing angular momentum is evident in the surface density profiles (the top left panel of Figure 3).

There appears to be a clear difference in trend between non-fragmenting discs (Simulations 1 and 2) and fragmenting discs (Simulations 3,4 and 5). In the non-fragmenting case, the surface density profile is visibly steeper (with a corresponding higher aspect ratio, seen in the top right panel). As these plots are time-averaged, we can use each snapshot to derive the standard deviations of each curve for all radii, and perform χ^2 fitting. All the curves are fitted to a power-law with exponential decay, of the form (Williams & Cieza 2011):

$$\Sigma(r) = \frac{(2-p)M_d}{2\pi R_c^2} \left(\frac{r}{R_c} \right)^{-p} \quad (16)$$

(where p and R_c are free parameters). This yields $p \sim 1.99$ for Simulation 1 and 2, and $p \sim 1$ for the other simulations. These results are reflected in the Toomre Q profiles in the bottom left panel, where Simulation 2 displays a very narrow range of gravitationally unstable radii in comparison to the other discs. Indeed, despite their apparent similarities in the rest of Figure 3, Simulations 3, 4 and 5 become distinct in their Q -profiles (although 3 and 4 remain similar). Simulation 5 displays the largest region of instability, extending over a range spanning approximately 80 au.

This set of results is an excellent example of disc fragmentation requiring at least two criteria be met. The bottom right panel shows the dimensionless cooling time parameter β_c , which again displays differing trends between fragmenting and non-fragmenting discs. Values of β_c of order unity present amenable conditions for fragmentation, and all four discs satisfy this condition in their outer edges. Simulation 2 satisfies this at the lowest radii, at around 40 au. However, we must also note that at 40 au, $Q \sim 3$ and is increasing with radius. Therefore, while this region can maintain very cool gas, it is not gravitationally unstable, and we therefore do not expect it to fragment - this expectation is satisfied, despite running the simulation for 30,000 years. As a test, we ran the disc for an extra 30,000 years, and no fragmentation was seen during this subsequent period.

The observant reader will note that fragments are able to form in Simulations 3 and 4 at large radii, despite high values of Q . Figure 4 goes some way to explaining this phenomenon. These discs are highly variable (Simulation 2 being the most steady-state of the four). While temperature fluctuations in these discs are relatively low, the fluctuations in Q are quite high, as has been observed previously in discs with infall (Harsono et al. 2011). Simulation 1 maintains fluctuations of order 50% in the outer regions, ensuring $Q \gg 2$. The other simulations have extremely high Q fluctuations (nearly 100%), and all possess very low values of β_c , of order unity or less. It is this transient behaviour that allows $Q < 2$ for a sufficient period of time (say one orbital period at a given radius) which allows the disc to fragment. Simulation 1 also has extremely variable Q , but this translates into relatively weak surface density perturbations in regions of low Σ (as can be seen in the left panel of Figure 4), and therefore does not fragment.

In effect, for Simulations 3 and 4 to fragment, the square of the epicyclic frequency must become negative, a phenomenon that typically defines the outer edge of accretion discs, where perturbations from circular flow will be unstable. This tends to agree with the consensus view that fragmentation in the inner regions of discs is difficult to achieve (Rafikov 2005; Matzner & Levin 2005; Whitworth & Stamatellos 2006; Boley et al. 2006; Stamatellos & Whitworth 2008; Forgan et al. 2009; Clarke 2009). On the other hand, Simulation 5 shows less variation than the others, and satisfies the canonical fragmentation criteria (see next section) at around 100 au, where fragments are subsequently seen. The initial fragment provides an extra torque to the spiral wave that spawned it, which results in consecutive fragmentation along the wave. For example, the condensation in the lower right quadrant of the lower right panel of Figure 2 subsequently fragments into several objects. In all the simulations conducted, if multiple fragmentation occurs, it seems to occur as a result of an initial fragment's torques on the disc, with time delays between the first object and the second object of up to an orbital period.

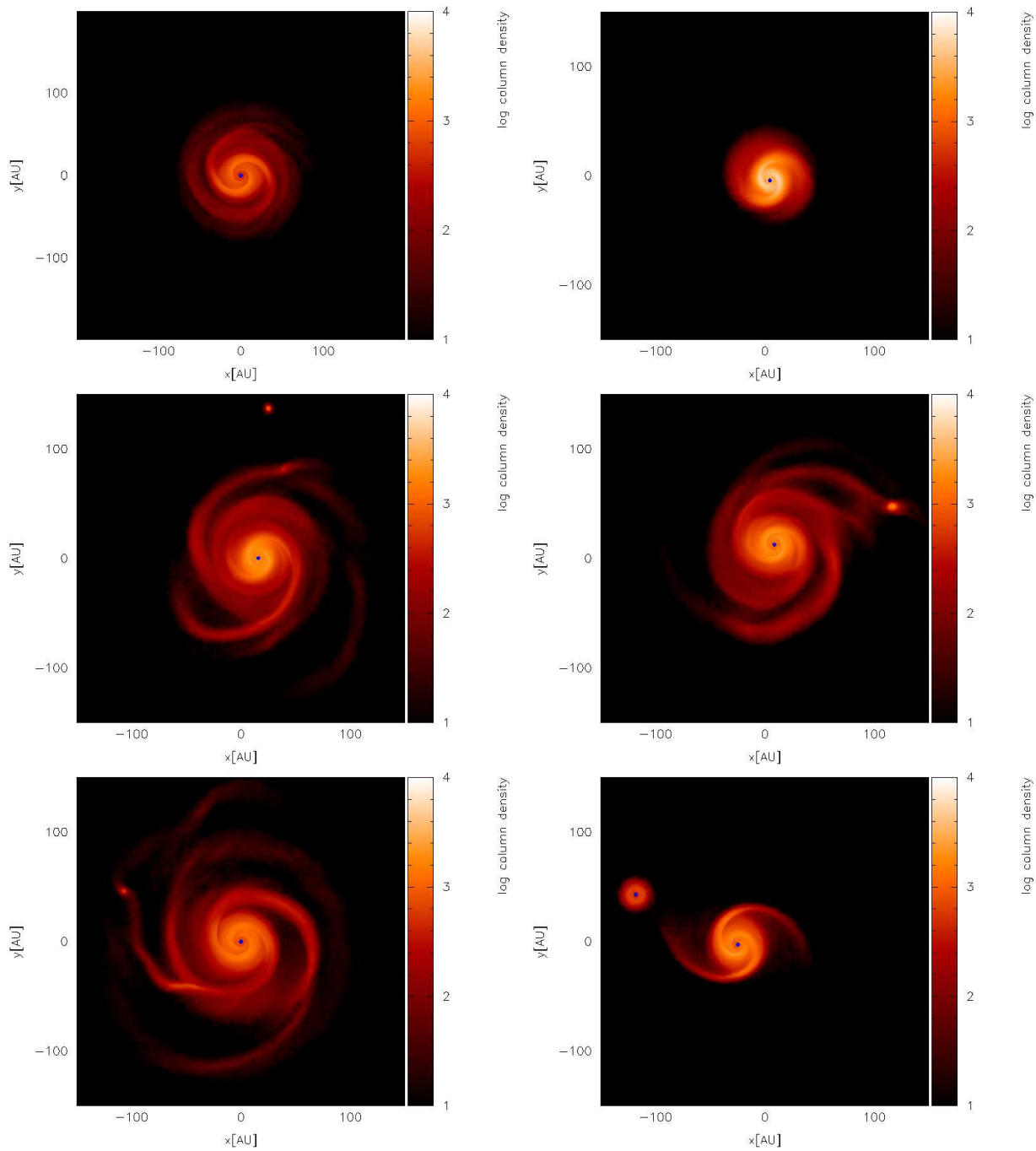


Figure 2. Surface density plots of the $M_{\text{cl}} = 1M_{\odot}$ simulations (Simulations 1, 2, 3, 4, 5 and 6). The snapshots were taken two free fall times after the collapse was initiated (for Simulations 1 and 2, top), or at the point of disc fragmentation (for Simulations 3, 4, 5 and 6, middle left and right, and bottom left and bottom right respectively).

3.2.2 Angular Momentum Transport

We have seen that the spiral structure appears to be dominated by $m = 2$ modes, and that the discs are highly variable. These are both symptoms of non-local angular momentum transport (Forgan et al. 2011), and have been seen in previous simulations with envelope accretion (Kratter et al. 2008; Harsono et al. 2011). We carried out a Fourier decomposition to study the amplitude of the m -modes. Figure 5 shows spectrally averaged m -modes as a function of disc position for Simulations 1-5. These confirm our visual inspection

of the discs' spiral structure - the dominant m -mode in the unstable region of all five discs is $m = 2$, with the majority of the power remaining in the lower modes at larger radii. However, Simulation 1 shows moderate power across a wide range of mode numbers³, suggesting that it may not be subject to non-local transport.

³ Spectral averaging weights the amplitude of each mode by m , giving rise to seemingly high average m modes as shown here - it is likely that $m \approx 4$ modes dominate in the case of Simulation 1.

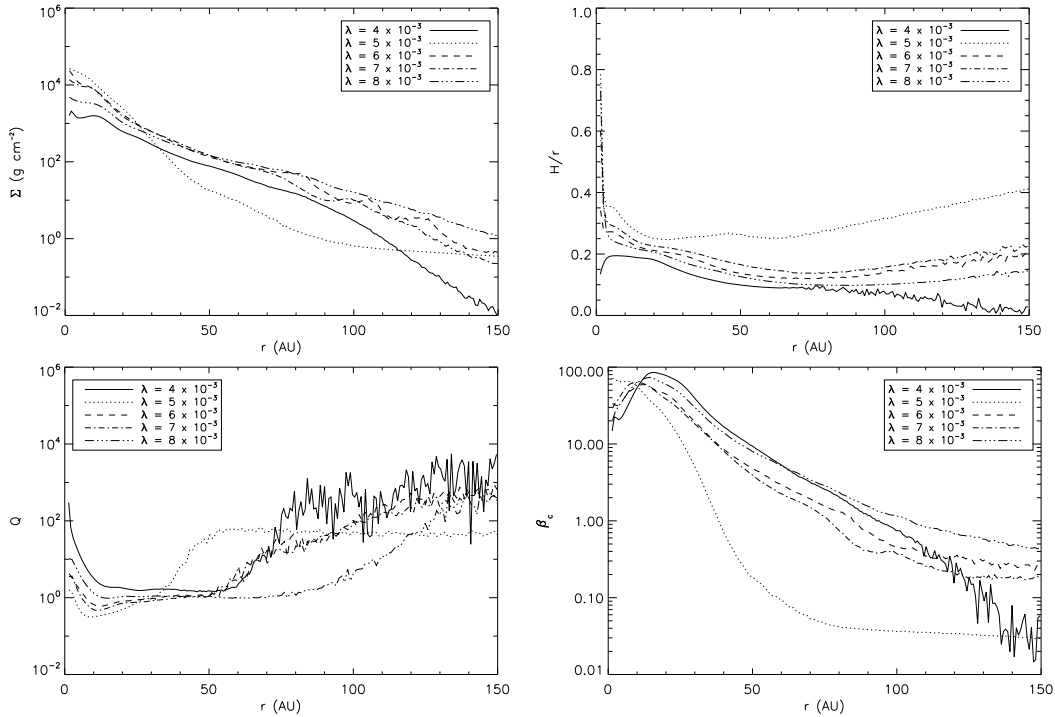


Figure 3. Azimuthally averaged radial profiles from the $M_{cl} = 1M_{\odot}$ simulations (Simulation 1 (solid line), Simulation 2 (dotted lines), Simulation 3 (dashed lines), Simulation 4 (dot-dashed lines) and Simulation 5 (triple-dot-dashed lines)). Simulation 6 is excluded as it forms a multiple system. The profiles are time averaged from the formation of the disc to the point of fragmentation (in the case of Simulations 1 and 2, they are time averaged for approximately 7000 years, corresponding to approximately 19 ORPs). The top left panel shows the surface density profile (calculated from the material contained within the first three scale heights only), the top right shows the aspect ratio, the bottom left shows the Toomre Q parameter, and the right hand panel shows β_c .

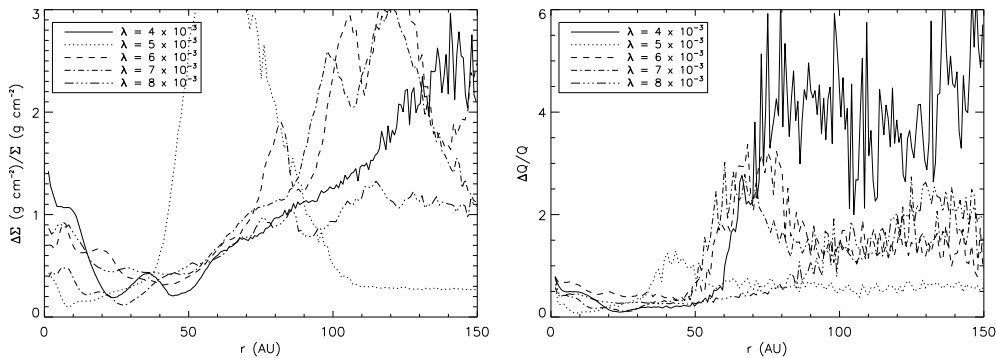


Figure 4. Variation in the mean surface density (left) and Toomre parameter Profile (right), for the $M_{cl} = 1.0M_{\odot}$ simulations (1, 2, 3, 4 and 5).

This is confirmed by calculating the non-local transport fraction ξ (Cossins et al. 2009; Forgan et al. 2011). All simulations except Simulation 1 exhibit values above 0.5, indicating non-local transport is significant. By contrast, Simulation 1 maintains values less than 0.2, indicating the transport is indeed local.

Figure 6 shows azimuthally averaged profiles of the α -parameter, calculated for various components of the disc stress. The solid lines indicate the total disc stress, the dashed lines show the contribution from gravitational stresses α_{grav} , and the dotted lines show the Reynolds stress α_{Reyn} (expressions for these functions can be found in Forgan et al. 2011). We also plot the stress induced by the artificial viscosity, α_{art} to confirm that it is small in comparison to the other disc stresses.

In contrast to isolated disc simulations, we can see that the

Reynolds stresses are typically large, of order $\alpha \sim 1$. This is in keeping with values obtained by Kratter et al. (2008) and Harsono et al. (2011) in similar disc configurations.

Again, there is a stark contrast between non-fragmenting and fragmenting discs. We can see that the standard $\alpha_{tot} = \alpha_{grav} + \alpha_{Reyn} > \alpha_{crit} = 0.06$ criterion (derived for isolated discs) is invalid. The large Reynolds stresses (induced by velocity shear from infalling envelope material contacting the disc's rotating flow) prevent the gravitational stress from dominating unless it can reach values closer to unity (in some cases up to 5 times larger than α_{crit}). We should therefore be careful about using this criterion in young systems that are still surrounded by a substantial envelope - indeed, we should develop new criteria that take this accretion into account (Forgan & Rice 2011).

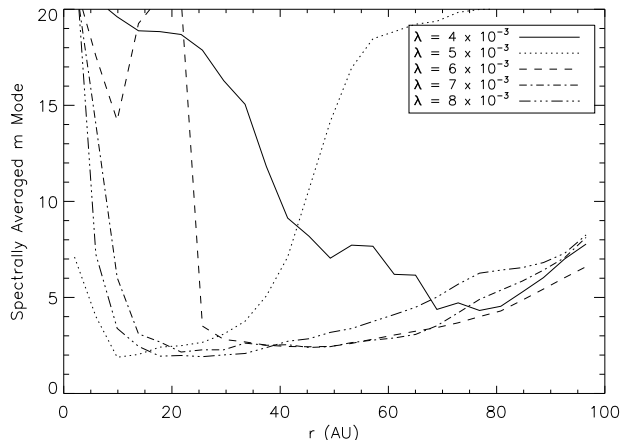


Figure 5. Spectrally averaged m modes as a function of radius for the $M_{\text{cl}} = 1.0M_{\odot}$ simulations (1, 2, 3, 4 and 5). Note that inside 10-20 au the discs are dominated by numerical viscosity, meaning that data in this region should be ignored. With the exception of Simulation 1, all discs exhibit non-local angular momentum transport. Consequently, the $m = 2$ mode dominates consistently at large radii for Simulations 2-5.

From this data, we suggest that fragmenting discs require the local gravitational stress to be of the order (or larger than) the local Reynolds stress. We can see that Simulation 2 satisfies this condition weakly at 40 au, again where Q is too large for the disc to be sufficiently unstable. At larger radii, the gravitational stress decreases with distance, further ensuring no fragmentation can occur. Simulation 1 appears to satisfy this at 100 au, but α_{grav} varies quite strongly, only dominating at much larger radii, where the surface density becomes negligible. The differences between Simulations 1 and 2 are due to the different modes of angular momentum transport at play (local and non-local respectively).

Simulations 3 and 4 show gravitational stresses comparable to local Reynolds stresses at around 150 and 110 au respectively - these correspond well to the initial formation radius of the fragments. Simulation 5 appears to be qualitatively different, in that it fragments in a regime where the gravitational stress is still small compared to the Reynolds stress, but $\alpha_{\text{grav}} > \alpha_{\text{crit}}$. The disc exhibits more power in higher m -modes than the others, and the total α -profile differs also. Where Simulations 3 and 4 show relatively flat α_{tot} outside 50 au, Simulation 5 shows a steadily increasing curve. Naively comparing with Forgan et al. (2011)'s study of isolated discs, this would suggest that Simulation 5 shows more evidence of local angular momentum transport than Simulations 3 and 4. However, as has been said, Simulations 3-5 all possess large non-local transport fractions.

Simulations 3-5 produce disc fragments at a minimum distance of 100 au from the central star, where the local (time-averaged) α_{grav} at the fragmentation radius ranges from 0.06 to 0.7. The subsequent evolution of the fragments in the non-linear regime vary between each simulation - for example, Simulations 3 and 5 produce several subsequent fragments each, as a result of torques induced by the presence of the initial fragment, which itself undergoes rapid inward migration. Simulation 4 produces a single fragment, which grows to form a second pointmass, where the mass ratio $M_2/M_1 \sim 0.15$.

4 DISCUSSION & CONCLUSION

From a set of numerical experiments with simplified initial conditions, we have shown that the initial cloud angular momentum tends to be the critical factor in subsequent disc fragmentation (compared to the initial thermal energy of the cloud). We confirm the results of Rice et al. (2010), in that fragmentation does not occur if $\lambda < 10^{-3}$. While they also state that fragmentation occurs if $\lambda > 10^{-3}$, their parameter study does not resolve the fragmentation boundary to the same level that this paper does. In this sense, we can say that their conclusions are broadly correct. Agreement can also be found on the fragmentation radius, which we also see increasing with initial cloud mass, and the steep surface density profiles obtained for non-fragmenting discs, placing a large amount of material within 20 au (although on this second statement we must caution that numerical effects dominate within 10 au). This agreement is somewhat surprising, in that they assume that the angular momentum transport due to self-gravity is local, where it has been established in this paper and in others that it is likely to be dominated by global spiral modes (cf Harsono et al. 2011).

All fragments form at distances above 70 au, typically consistent with previous studies of both isolated and accreting discs (Rafikov 2005; Matzner & Levin 2005; Whitworth & Stamatellos 2006; Boley et al. 2006; Stamatellos & Whitworth 2008; Forgan et al. 2009; Clarke 2009; Rice et al. 2010), which indicate that, despite maintaining low values of Q , the inner regions do not cool efficiently or impart sufficient stress due to the gravitational instability to produce fragments. This is true in spite of non-local angular momentum transport or accretion from the envelope. It appears that maintaining surface density profiles which place large amounts of (cool) material at large enough radii is the key to fragmentation. The disc-to-star mass ratios are typically of order 0.5 at fragmentation, although they can be lower (cf Stamatellos et al. 2011). The masses of fragments formed are typically range from 1 to 15 Jupiter masses: these are roughly consistent with the local Jeans mass in the spiral waves from which they form (Forgan & Rice 2011), except in some cases where the Jeans length is sufficiently long to allow the break up of fragments into multiple objects. Future work will focus on the survival of such fragments as they condense out of the disc, to investigate the role of internal pressure support (Kratter & Murray-Clay 2011) and the importance of fragment-fragment collisions (Shlosman & Begelman 1989).

Marginally unstable, self-gravitating discs which do not fragment can remain massive for long periods of time. In one case, the disc was shown to remain at masses roughly half that of the parent star for around 50,000 years after formation, showing that the self-gravitating phase could be more long-lasting than previously thought, much as the Class 0 and Class I timescales have also been shown to be much longer than expected (Evans 2011).

The inherent variability seen in all simulations conducted indicates that accretion onto the central star varies significantly. Even in the more quiescent, non-fragmenting simulations, the value of Q varies by up to 50% or more, ensuring episodes of gravitational instability marked by high-amplitude, low- m spiral waves followed by episodes of relative stability with weak spiral structures. This variability occurs despite the omission of stellar radiative feedback physics, unlike e.g. Stamatellos et al. (2011), who demonstrate that accretion luminosity can enhance this episodic nature of instability. This would suggest that self-gravity alone may account for the variability seen in Class I protostars (Boley & Durisen 2008; Vorobyov 2009). It is quite possible that the one-parameter boundary we find

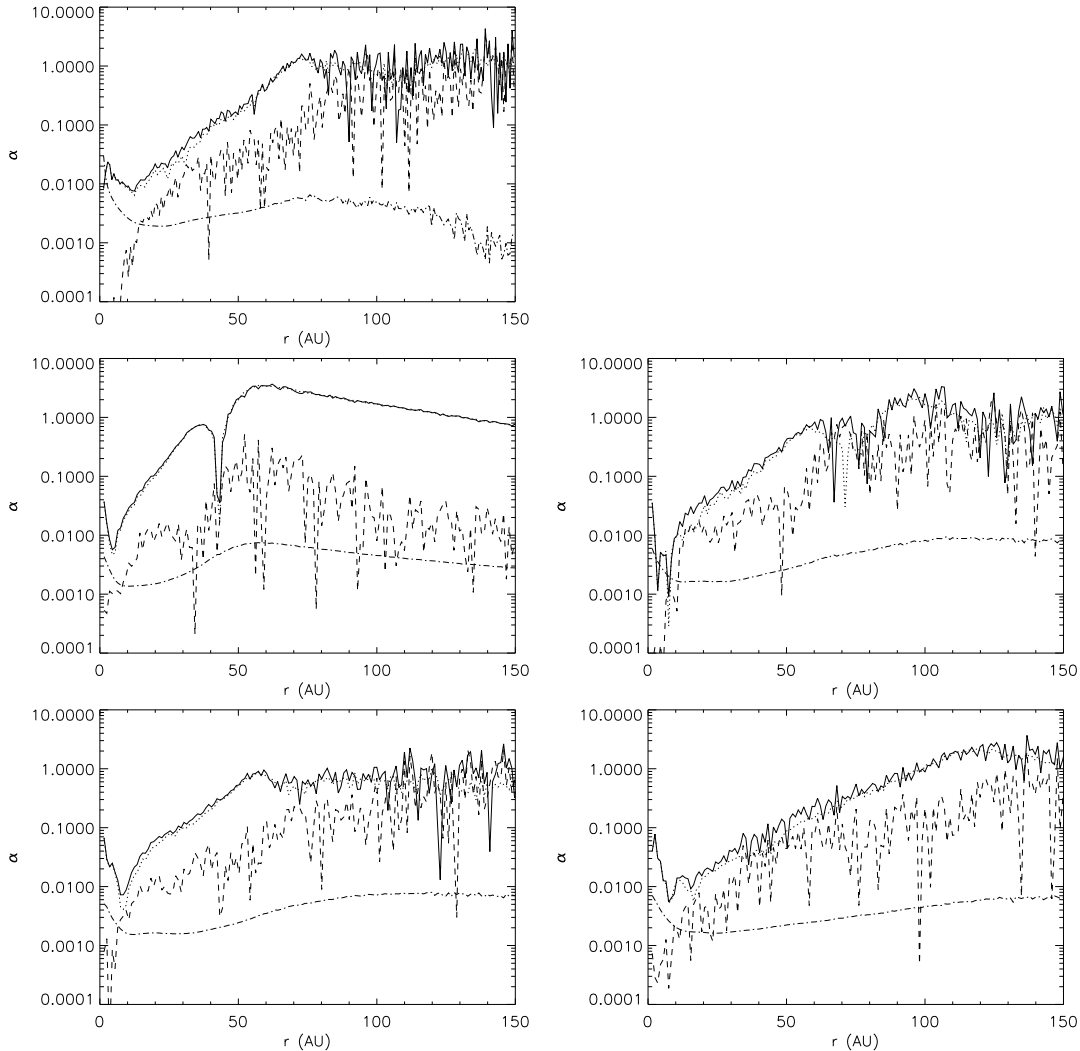


Figure 6. Azimuthally averaged α -parameter for the $M_{\text{cl}} = 1M_{\odot}$ simulations (Simulation 1 (top left panel), Simulation 2 (top right panel), Simulation 3 (bottom left panel) and Simulation 4 (bottom right panel)). Simulation 5 is excluded as it forms a multiple system. The profiles are time averaged from the formation of the disc to the point of fragmentation (in the case of Simulation 1, it is time averaged for 7000 years, corresponding to approximately 19 ORPs). The solid line shows the total α , the dashed lines show α_{grav} , the dotted lines show α_{Reyn} , and the dot-dashed lines show the contribution to the stress from artificial viscosity, α_{art} . Note that this numerical α dominates within around 10 AU, so we must disregard data from within this region.

disappears with the addition of stellar luminosity, as its strength will clearly depend on M_{cl} .

Indeed, this simple boundary is unlikely to apply in nature due to other complicating factors, including non-uniform density profiles and the addition of turbulence. A density profile that decays with radius, such as a supercritical Bonnor-Ebert sphere is a more physical choice, ensuring more mass will be concentrated in the inner disc at early times. We suggest that these steeper profiles will require an increased amount of initial angular momentum to produce fragmentation, and that the boundary established for uniform clouds is a lower limit⁴.

The addition of turbulence tends to weaken any correlation with angular momentum (Walch et al. 2010). Spherical symmetry is broken by construction, and discs accrete from the environment

through filamentary structures, allowing significant specific angular momentum to be injected asymmetrically, exciting low- m spiral modes as the disc attempts to redistribute itself. In general, discs formed from turbulent simulations tend to grow more slowly, and have smaller radii for a given angular momentum - this again suggests that the criterion derived in this paper remains a lower limit.

Considering that the threshold angular momentum required ($\lambda \gtrsim 5 \times 10^{-3}$) is small compared to observations, which indicate a median of $\lambda \sim 0.02$ (Goodman et al. 1993) - this would suggest that disc fragmentation will be a somewhat common process, but occur on such short timescales that observations of such events will be rare (Stamatellos et al. 2011). Exactly how this threshold might vary with surface density profile and the addition of turbulence is difficult to quantify, but merits further research.

⁴ Strictly, an even lower limit could exist if the density increased with radius, but these conditions are even less likely to appear in nature than simple uniform conditions

ACKNOWLEDGMENTS

Density plots were produced using SPLASH (Price 2007). All simulations were performed using high performance computing funded by the Scottish Universities Physics Alliance (SUPA). DF and KR gratefully acknowledge support from STFC grant ST/H002380/1.

REFERENCES

- Artymowicz P., Lubow S. H., 1994, *ApJ*, 421, 651
 Balbus S. A., Papaloizou J., 1999, *ApJ*, 521, 650
 Bate M. R., 2010, *MNRAS*, 404, L79
 Bate M. R., Bonnell I. A., Price N. M., 1995, *MNRAS*, 277, 362
 Bate M. R., Burkert A., 1997, *MNRAS*, 288, 1060
 Bell K. R., Lin D. N. C., 1994, *ApJ*, 427, 987
 Blaes O. M., Balbus S. A., 1994, *ApJ*, 421, 163
 Boley A. C., Durisen R., 2008, *ApJ*, 685, 1193
 Boley A. C., Hartquist T. W., Durisen R. H., Michael S., 2007, *ApJ*, 656, L89
 Boley A. C., Mejia A. C., Durisen R., Cai K., Pickett M. K., D'Alessio P., 2006, *ApJ*, 651, 517
 Boss A. P., 1984, *Royal Astronomical Society*, 209, 543
 Boss A. P., 1997, *Science*, 276, 1836
 Boss A. P., 1986, *The Astrophysical Journal Supplement Series*, 62, 519
 Cai K., Durisen R., Boley A. C., Pickett M. K., Mejia A. C., 2008, *ApJ*, 673, 1138
 Caselli P., Benson P. J., Myers P. C., Tafalla M., 2002, *The Astrophysical Journal*, 572, 238
 Clarke C. J., 2009, *MNRAS*, 396, 1066
 Clarke C. J., Harper-Clark E., Lodato G., 2007, *MNRAS*, 381, 1543
 Clarke C. J., Lodato G., 2009, *MNRAS*, 398, L6
 Cossins P., Lodato G., Clarke C. J., 2009, *MNRAS*, 393, 1157
 Durisen R., Boss A. P., Mayer L., Nelson A. F., Quinn T., Rice W. K. M., 2007, in Reipurth B., Jewitt D., Keil K., eds, *Protostars and Planets V Gravitational Instabilities in Gaseous Protoplanetary Disks and Implications for Giant Planet Formation*. University of Arizona Press
 Evans N. J., 2011, *Proceedings of the International Astronomical Union*, 6, 25
 Forgan D., Rice K., 2011, *MNRAS*, p. in press
 Forgan D., Rice K., Cossins P., Lodato G., 2011, *MNRAS*, 410, 994
 Forgan D. H., Rice K., Stamatellos D., Whitworth A. P., 2009, *MNRAS*, 394, 882
 Gammie C., 2001, *ApJ*, 553, 174
 Gingold R. A., Monaghan J. J., 1977, *MNRAS*, 181, 375
 Goodman A. A., Benson P. J., Fuller G. A., Myers P. C., 1993, *ApJ*, 406, 528
 Harsono D., Alexander R. D., Levin Y., 2011, *MNRAS*, 413, 423
 Kratter K. M., Matzner C. D., Krumholz M. R., 2008, *ApJ*, 681, 375
 Kratter K. M., Murray-Clay R. A., 2011, *ApJ*, p. in press
 Kratter K. M., Murray-Clay R. A., Youdin A. N., 2010, *ApJ*, 710, 1375
 Kuiper G. P., 1951, *Proceedings of the National Academy of Sciences*, 37, 1
 Larson R. B., 1969, *MNRAS*, 145
 Laughlin G., Bodenheimer P., 1994, *ApJ*, 436, 335
 Lin D. N. C., Pringle J. E., 1987, *MNRAS*, 225, 607
 Lin D. N. C., Pringle J. E., 1990, *ApJ*, 358, 515
 Lodato G., Clarke C. J., 2011, *MNRAS*, 413, 2735
 Lodato G., Price D. J., 2010, *MNRAS*, 405, 1212
 Lodato G., Rice W. K. M., 2004, *MNRAS*, 351, 630
 Lucy L. B., 1977, *The Astronomical Journal*, 82, 1013
 Machida M. N., Matsumoto T., 2011, *MNRAS*, 413, 2767
 Masunaga H., Inutsuka S., 2000, *ApJ*, 531, 350
 Matzner C. D., Levin Y., 2005, *ApJ*, 628, 817
 Mayer L., Lufkin G., Quinn T., Wadsley J., 2007, *ApJ*, 661, L77
 Meru F., Bate M. R., 2011a, *MNRAS*, 411, L1
 Meru F., Bate M. R., 2011b, *MNRAS*, 410, 559
 Monaghan J. J., 1992, *ARA&A*, 30, 543
 Monaghan J. J., 2005, *Reports on Progress in Physics*, 68, 1703
 Murray J. R., 1996, *MNRAS*, 279, 402
 Nero D., Bjorkman J. E., 2009, *ApJ*, 702, L163
 Paardekooper S.-J., Baruteau C., Meru F., 2011, *MNRAS*, 416, L65
 Paczynski B., 1978, *Acta Astronomica*, 28, 91
 Pickett B. K., Mejia A. C., Durisen R., Cassen P. M., Berry D. K., Link R. P., 2003, *ApJ*, 590, 1060
 Price D. J., 2007, *PASA*, 24, 159
 Rafikov R., 2005, *ApJ*, 621, 69
 Rice W. K. M., Armitage P. J., 2009, *MNRAS*, 396, 2228
 Rice W. K. M., Armitage P. J., Mamatsashvili G. R., Lodato G., Clarke C. J., 2011, eprint arXiv:1108.1194
 Rice W. K. M., Lodato G., Armitage P. J., 2005, *MNRAS*, 364, L56
 Rice W. K. M., Lodato G., Pringle J. E., Armitage P. J., Bonnell I. A., 2004, *MNRAS*, 355, 543
 Rice W. K. M., Mayo J. H., Armitage P. J., 2010, *MNRAS*, 402, 1740
 Shakura N. I., Sunyaev R. A., 1973, *A&A*, 24, 337
 Shlosman I., Begelman M. C., 1989, *ApJ*, 341, 685
 Stamatellos D., Hubber D. A., Whitworth A. P., 2007, *MNRAS*, 382, L30
 Stamatellos D., Maury A., Whitworth A., André P., 2011, *MNRAS*, 413, 1787
 Stamatellos D., Whitworth A. P., 2008, *A&A*, 480, 879
 Stamatellos D., Whitworth A. P., Bisbas T., Goodwin S., 2007, *A&A*, 475, 37
 Stamatellos D., Whitworth A. P., Hubber D. A., 2011, *The Astrophysical Journal*, 730, 32
 Terebey S., Shu F. H., Cassen P., 1984, *The Astrophysical Journal*, 286, 529
 Tohline J. E., 1981, *ApJ*, 248, 717
 Toomre A., 1964, *ApJ*, 139, 1217
 Vorobyov E. I., 2009, *The Astrophysical Journal*, 704, 715
 Walch S., Burkert A., Whitworth A., Naab T., Gritschneider M., 2009, *MNRAS*, 400, 13
 Walch S., Naab T., Whitworth A., Burkert A., Gritschneider M., 2010, *MNRAS*, 402, 2253
 Whitehouse S. C., Bate M. R., 2004, *MNRAS*, 353, 1078
 Whitworth A. P., 1998, *MNRAS*, 296, 442
 Whitworth A. P., Stamatellos D., 2006, *A&A*, 458, 817
 Williams J. P., Cieza L. A., 2011, eprint arXiv:1103.0556